Opto-Electronic Advances

Supplementary information

May 2024, Vol. 7, No. 5

DOI: 10.29026/oea.2024.230145

Towards the performance limit of catenary meta-optics via field-driven optimization

Siran Chen[1,2,3†], Yingli Ha[1,2,4†], Fei Zhang[1,2,4], Mingbo Pu[1,2,3,4*], Hanlin Bao[1,2,3], Mingfeng Xu[1,2,4], Yinghui Guo[1,2,3,4], Yue Shen[5], Xiaoliang Ma[1,2,3], Xiong Li[1,2,3] and Xiangang Luo[1,2*]

[1]National Key Laboratory of Optical Field Manipulation Science and Technology, Chinese Academy of Sciences, Chengdu 610209, China; [2]State Key Laboratory of Optical Technologies on Nano-Fabrication and Micro-Engineering, Institute of Optics and Electronics, Chinese Academy of Sciences, Chengdu 610209, China; [3]College of Materials Science and Opto-Electronic Technology, University of Chinese Academy of Sciences, Beijing 100049, China; [4]Research Center on Vector Optical Fields, Institute of Optics and Electronics, Chinese Academy of Sciences, Chengdu 610209, China; [5]Department of Electrical and Computer Engineering, University of California Los Angeles (UCLA), Los Angeles, California 90095, USA.

[†]These authors contributed equally to this work.

*Correspondence: MB Pu, E-mail: pmb@ioe.ac.cn; XG Luo, E-mail: lxg@ioe.ac.cn

This file includes:

Supplementary information for this paper is available at https://doi.org/10.29026/oea.2024.230145

Section 1: Theory of the field-driven optimization (FDO)

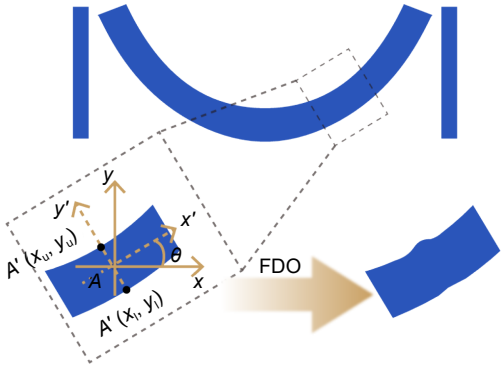

Fig. S1 | Schematic of an FDO process. Different from the adjoint-based shape optimization, FDO is utilized to optimize the width of each point along the trajectory of the catenary structure.

The optimization process of FDO starts by defining the FoM, which could be defined as the fraction of the output field $\boldsymbol{E}^{\mathrm{f}}$ in the ideal field distribution $\boldsymbol{E}_{\mathrm{ideal}}$[S1]:

$$FoM = \left|\left\langle \boldsymbol{E}_{\mathrm{ideal}} \middle| \boldsymbol{E}^{\mathrm{f}} \right\rangle\right|^2 , \tag{S1}$$

The subsequent imperative step involves acquiring the variation of the FoM with respect to the width w, which requires conducting another simulation, namely adjoint simulation. In the adjoint simulation, the structures remain identical to that in the forward simulation. The adjoint source is set as $\partial FoM / \partial E^{f}$[S2], while the resultant electric field acquired from the adjoint simulation is referred to as $\boldsymbol{E}^{A}$. If the FoM is given as Eq. (S1), according to the symmetry of the Maxwell-Green's function, the adjoint source can be set as an electromagnetic wave with electric field $\boldsymbol{E}_{\mathrm{ideal}}{}^{*}$[S1], where * indicates the conjugate. Different from the proposed adjoint-based shape optimization algorithm, which optimizes the width and length of the rectangular structure, the proposed FDO method aims to optimize the width of each point on the trajectory of the structure individually. As shown in Fig. S1, assuming the coordinates of point A on the structural trajectory are (x, y), thus the orientation angle of point A is θ=tan$^{-1}(y/x)$. The coordinates of the corresponding points on the boundary are $(x_{\mathrm{u/l}}, y_{\mathrm{u/l}})$. Then, based on the Lorentz reciprocity theorem, the partial derivative of FoM with respect to the width $w_{\mathrm{u,l}}$ at point A is expressed as[S3]:

$$\delta FOM = 2\mathrm{Re}\left\{(\varepsilon_2 - \varepsilon_1)\left[\boldsymbol{E}^{A}_{x'}(x_{\mathrm{u,l}}, y_{\mathrm{u,l}})\boldsymbol{E}^{\mathrm{f}}_{x'}(x_{\mathrm{u,l}}, y_{\mathrm{u,l}}) + \frac{\boldsymbol{D}^{A}_{y'}(x_{\mathrm{u,l}}, y_{\mathrm{u,l}})\boldsymbol{D}^{\mathrm{f}}_{y'}(x_{\mathrm{u,l}}, y_{\mathrm{u,l}})}{\varepsilon_1\varepsilon_2}\right]\right\}\delta w_{\mathrm{u,l}} , \tag{S2}$$

where ε_1 and ε_2 denote the dielectric constants of the environment and the structures, respectively. $\delta w_{\mathrm{u,l}}$ indicates the upper and lower width gradient of the point A. $\boldsymbol{E}_{x',y'}$ and $\boldsymbol{D}_{x',y'}$ represent the components of the electric field and electric displacement vector along the x' and y' direction, which is tangent and normal to the trajectory of the structure as shown in Fig. S1:

$$\begin{bmatrix} \boldsymbol{E}_{x'} & \boldsymbol{E}_{y'} \end{bmatrix}^{\mathrm{T}} = \boldsymbol{R}(\theta)\begin{bmatrix} \boldsymbol{E}_{x} & \boldsymbol{E}_{y} \end{bmatrix}^{\mathrm{T}} , \tag{S3}$$

where $\boldsymbol{E}_x$ and $\boldsymbol{E}_y$ are the x and y component of the electric field obtained by the two simulations, and $\mathbf{R}(\theta)$ denotes the coordinate transformation matrix. Finally, to ensure that the first order the merit function increases each iteration, the gradient of each point at structures could be set as[S4]:

$$\delta w_{\mathrm{u,l}} = \mathrm{Re}\left\{(\varepsilon_2 - \varepsilon_1)\left[\boldsymbol{E}^{A}_{x'}(x_{\mathrm{u,l}}, y_{\mathrm{u,l}})\boldsymbol{E}^{\mathrm{f}}_{x'}(x_{\mathrm{u,l}}, y_{\mathrm{u,l}}) + \frac{\boldsymbol{D}^{A}_{y'}(x_{\mathrm{u,l}}, y_{\mathrm{u,l}})\boldsymbol{D}^{\mathrm{f}}_{y'}(x_{\mathrm{u,l}}, y_{\mathrm{u,l}})}{\varepsilon_1\varepsilon_2}\right]\right\} , \tag{S4}$$

It's worth noting that the above method is a general framework that is not constrained by the polarization state of the incident light, incident angle, wavelength or the desired functionality of the devices.

Section 2: Top view of the initial and optimized structures.

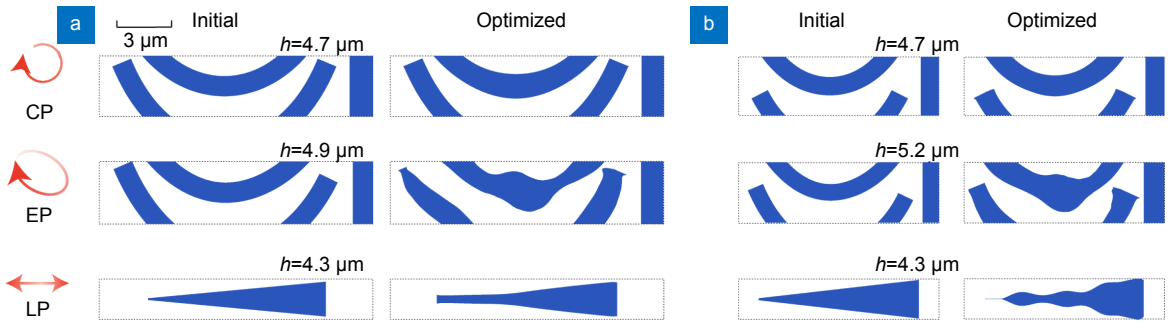

Fig. S2 | The dimensions and heights (*h*) of the initial and shape-optimized structures with diffraction angles of (a) 45° and (b) 75°.

Section 3: The broadband performance of the periodic devices.

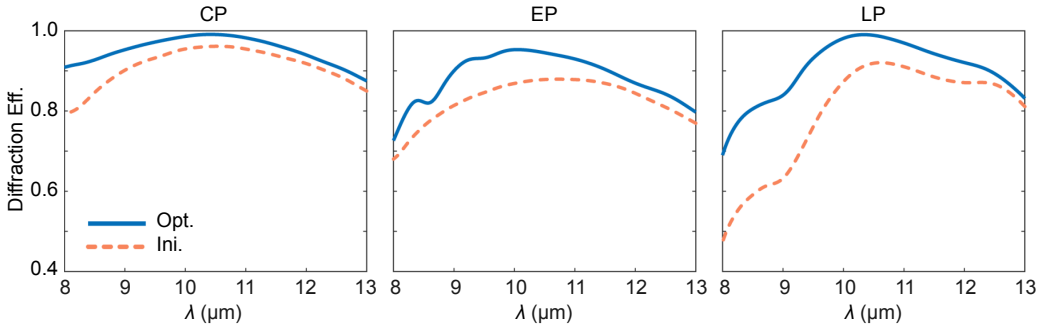

Fig. S3 | The broadband performance of the periodic devices with diffraction angles of 45° with light incidence of 10.6 μm

Although, the performances of the devices are optimized at the wavelength of 10.6 μm, a discernible improvement in performance is evident across the broadband of 8–13 μm. The average diffraction efficiencies within 8–13 μm of the devices designed for CP, EP, and LP light improve from 90.6%, 82.29% and 76.61% to 95.27%, 88.54%, and 89.42%, respectively. Here, we perform equal-frequency sampling of the devices' performances within 8–13 μm, comprising a total of 201 sampling points. The averaging diffraction efficiency is defined as the average value of these 201 diffraction efficiencies. For the shape-optimized catenary structure which is designed for CP incidence, the suppression of the wavelength dependent parasitic propagation phase makes it maintain excellent performance across the broadband. By optimizing the devices for light incidence with different wavelengths, the broadband performances of the devices may be further enhanced.

Section 4: Experimental setup

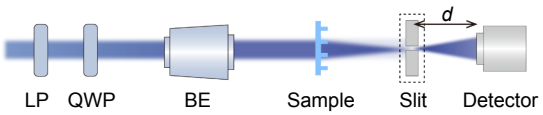

Fig. S4 | The schematic of experimental setup for detecting the efficiencies and light intensity distributions of the designed metalenses.

Figure S4 shows the experimental setup for detecting the efficiencies and the light intensity distributions of the samples. The laser is modulated by the linear polarizer (LP) and quarter-wave plate (QWP), then illuminates the sample with a beam expander (BE). An optical slit is placed at the focal plane to filter out the focused light. The power of the focused light P_f is detected by a large-target power detector (diameter: 55 mm) with a distance of $d \approx 0.5$ cm to ensure that all the focused light is detected. Then, the slit is removed to measure the power of the transmitted lights P_t. The experimental focusing efficiency is defined as P_f/P_t. Here d represents the distance between the detector and the focal plane. To measure the zero-order efficiency, the slit is removed, and the distance between the detector and the focal plane is set as $d \approx$

25 cm. The efficiency of zero-order is defined as P_z/P_t, where P_z is the power of the zero-order. According to our measurement method, the theoretical experimental focusing efficiencies for these metalenses all exceed 99.9%, while the zero-order efficiency is all less than 0.1%. The theoretical experimental focusing efficiencies for the metalenses with *NA*=0.3, 0.4, and 0.5 are 99.92% (Exp: 90.8% and 79.1%), 99.94% (Exp: 94.6% and 81.3%) and 99.96% (Exp: 94.7% and 86.7%), respectively. To align with the experimental focusing efficiency definition, the theoretic prediction focusing efficiency is defined as the ratio of the power of the diffracted field within a 0.5 mm range from the center of the focal spot and the total transmitted light on the focal plane. In order to obtain the ideal light intensity distribution on the focal plane, an ideal metalens is illuminated with a plane wave, followed by calculating the light intensity distribution on the focal plane using the vector angular spectrum theory. To detect the light intensity distribution on the focal plane, the slit is removed, and a charge coupled device (CCD, pixel size: 17 μm × 17 μm) camera is placed on an electric moving stage.

Section 5: The definitions of the mentioned efficiencies.

Table S1 | The definitions of the mentioned efficiencies and energy.

Efficiencies	Subject to assessment	Definitions
Diffraction efficiency (DifEff)	Deflectors	P_m/P_t
Focusing efficiency (FocEff)	Metalenses (Sim.)	$P_{3FHWM}/(P_t$·Ideal-FocEff)
Ideal-FocEff	Metalenses (Sim.)	The ideal FocEff
Absolute efficiency	Deflectors/ Metalenses (Sim.)	DifEff(FocEff)·P_t/P_{in}
Experimental FocEff	Metalenses (Exp.)	P_f/P_t
Zero-order efficiency	Metalenses (Exp.)	P_z/P_t

P_m (power of the light at the target diffraction order); P_t (power of the transmitted light); P_{in} (power of the incident light); P_{3FHWM} (power of the light within a range of 3 times the FHWM on the focal plane); P_f (power of the focused light); P_z (power of the zero-order light)

To demonstrate the excellence of our work, we compared the performance of transmissive dielectric catenary structures operating at 10.6 μm, as shown in Table S2:

Table S2 | Comparation of the diffraction efficiency of the dielectric catenary structures operating at 10.6 μm.

No.	The optimization method	Diffraction efficiency
1[S5]	Equal-width catenary	96.94%
2[S6]	Equal-width catenary	~97%
3[S7]	Periodic boundary approximation-based optimization algorithm	98.4%
Our	Real boundary based FDO optimization algorithm	99.2%

Catenary structures serve as fundamental components for optical devices such as deflectors and metalenses. High-efficiency foundational structures play a crucial role in designing functional devices with high-performance. For instance, a catenary structure severs as a supercell of a deflector. Thus, the efficiency of the catenary directly impacts the performance of the deflector. Furthermore, a combination of a group of catenary structures forms a metalens, where high-efficiency catenary structures significantly enhance its performance. Our research has demonstrated that improving the diffraction efficiency of catenary structures has led to a notable ~15% increase in the focusing efficiency of metalenses.

References

S1. Xu MF, Pu MB, Sang D, Zheng YH, Li X et al. Topology-optimized catenary-like metasurface for wide-angle and high-efficiency deflection: from a discrete to continuous geometric phase. *Opt Express* **29**, 10181–10191 (2021).

S2. Liu YJ, Zhang F, Xie T, Pu MB, Zhao ZY et al. Polarization-multiplexed metalens enabled by adjoint optimization. *Chin Opt* **14**, 754–763 (2021).

S3. Mansouree M, McClung A, Samudrala S, Arbabi A. Large-scale parametrized metasurface design using adjoint optimization. *ACS Photonics* **8**, 455–463 (2021).

S4. Miller OD. *Photonic Design: From Fundamental Solar Cell Physics to Computational Inverse Design* (University of California, Berkeley, 2012).

S5. Zhang F, Zeng QY, Pu MB, Wang YQ, Guo YH et al. Broadband and high-efficiency accelerating beam generation by dielectric catenary

metasurfaces. *Nanophotonics* **9**, 2829–2837 (2020).

S6. Zhang YX, Pu MB, Guo YH, Jin JJ, He Q et al. High-efficiency mid-infrared catenary metasurface for chiral spectrometer. *Proc SPIE* **120720**, 120720F (2021).

S7. Zhang F, Pu MB, Li X, Ma XL, Guo YH et al. Extreme-angle silicon infrared optics enabled by streamlined surfaces. *Adv Mater* **33**, 2008157 (2021).